


Fock-space relativistic coupled-cluster calculation of a hyperfine-induced $^1S_0 \rightarrow ^3P_0^o$ clock transition in Al^+

Ravi Kumar,¹ S. Chattopadhyay,² D. Angom,³ and B. K. Mani¹

¹*Department of Physics, Indian Institute of Technology, Hauz Khas, New Delhi 110016, India*

²*Department of Physics, Kansas State University, Manhattan, Kansas 66506, USA*

³*Physical Research Laboratory, Ahmedabad 380009, Gujarat, India*

 (Received 16 March 2020; revised 7 January 2021; accepted 7 January 2021; published 1 February 2021)

We have developed an all-particle Fock-space relativistic coupled-cluster method to calculate the properties of two-valence atoms and ions. Using the method we compute the properties associated with a hyperfine-induced $^1S_0 \rightarrow ^3P_0^o$ clock transition in Al^+ . Our result of the $^3P_0^o$ metastable-state lifetime, 20.20 ± 0.91 s, is in excellent agreement with the experimental value, 20.60 ± 1.4 s [T. Rosenband *et al.*, *Phys. Rev. Lett.* **98**, 220801 (2007)]. Our studies show that the contributions from the triple excitations, and the corrections from the Breit interaction and QED effects, are essential to obtain accurate clock properties in Al^+ .

DOI: [10.1103/PhysRevA.103.022801](https://doi.org/10.1103/PhysRevA.103.022801)

I. INTRODUCTION

Development of atomic clocks as a frequency standard provides a road map to study fundamental as well as technological applications. Some important examples are the variation of the fundamental constants, probing physics beyond the standard model of particle physics, navigation systems, and the basis for the redefinition of the second [1–4]. The recent frequency standard experiments [5–9] in the optical domain have reported the $^1S_0 \rightarrow ^3P_0^o$ transition in Al^+ as one of the most accurate clock transitions. Though the $^1S_0 \rightarrow ^3P_0^o$ transition is highly forbidden based on the selection rule of the total electronic angular momentum J , it is possible through hyperfine mixing of the $^3P_0^o$ state with $^3P_1^o$ and $^1P_1^o$ states. The lifetime of the $^3P_0^o$ metastable clock state was measured with high accuracy by Rosenband and collaborators [5] using the quantum logic spectroscopy technique. Three key factors favoring the choice for this transition as a clock transition are low sensitivity to electromagnetic fields, narrow natural linewidth, and small room-temperature blackbody radiation shift. The last is due to small difference between the polarizabilities of 1S_0 and $^3P_0^o$ states [10,11]. A recent work reported the fractional frequency uncertainty of a ($^1S_0 \rightarrow ^3P_0^o$)-transition-based Al^+ clock as 9.4×10^{-19} [8]. And, this, perhaps, is the most precise atomic clock in existence today.

Despite the important applications of the $^1S_0 \rightarrow ^3P_0^o$ hyperfine-induced electric dipole transition ($E_{1\text{HFS}}$) and several experimental investigations in progress, very little theoretical data on the associated properties are available. For example, there are only two results on the lifetime of the $^3P_0^o$ metastable clock state [12,13], and both are based on the multiconfiguration Dirac-Fock (MCDF) method. To the best of our knowledge, there are no theoretical results using the accurate many-body methods like the relativistic coupled-cluster (RCC) method. It is to be emphasized that the RCC

method is considered to be one of the most accurate many-body theories for the structure and properties calculations of atoms and ions. It accounts for the electron correlation effects to all orders of residual Coulomb interaction, and has been employed to obtain accurate properties in several closed-shell and one-valence atoms and ions [14–17]. The implementation of the RCC method for two-valence atomic systems is, however, limited to few studies [18–20]. The reason, perhaps, is the complications associated with its implementation for two-valence systems. To be more precise, there are three main hurdles. First, due to the multireference nature of the configuration space, the model wave function is not well defined. This needs a special treatment through the diagonalization of the effective Hamiltonian matrix. Second, the atomic states are the eigenstates of the total angular momentum, which leads to a complication in the angular factors associated with antisymmetrized many-electron states. And third, there is divergence due to *intruder* states.

It can thus be surmised that there is a clear research gap in terms of the scarcity of accurate theoretical data on the $^1S_0 \rightarrow ^3P_0^o$ transition properties. The aim of this work is to fill this research gap. To address this in a comprehensive way, we adopt a three-pronged approach. First, we develop a Fock-space relativistic coupled-cluster (FSRCC)-based method for structure and properties calculations of two-valence atoms or ions. Second, we implement it as a parallel code. This is used to compute the properties, such as the excitation energies, hyperfine structure (HFS) constants, oscillator strengths, and, more importantly, the lifetime of the $^3P_0^o$ clock state, associated with the $^1S_0 \rightarrow ^3P_0^o$ clock transition in Al^+ . And, third, we examine in the detail the role and contributions of triple excitations, Breit interaction, and QED corrections in these properties.

The remaining part of the paper is divided into five sections. In Sec. II, we discuss the FSRCC method for two-valence atomic systems. The properties calculations using the

two-valence FSRCC method and contributing diagrams are discussed in Sec. III. The results obtained from our calculations are discussed and analyzed in Sec. IV. In Sec. V, we discuss the theoretical uncertainty of our results. Unless stated otherwise, all results and equations presented in this paper are in atomic units ($\hbar = m_e = e = 1/4\pi\epsilon_0 = 1$).

II. TWO-VALENCE FSRCC

The wave function of a two-valence atom or ion, $|\Psi_{vw}\rangle$, is the solution of the eigenvalue equation

$$H^{\text{DCB}}|\Psi_{vw}\rangle = E_{vw}|\Psi_{vw}\rangle, \quad (1)$$

where E_{vw} is the exact energy. The Hamiltonian H^{DCB} is the Dirac-Coulomb-Breit no-virtual-pair Hamiltonian,

$$H^{\text{DCB}} = \sum_{i=1}^N [c\alpha_i \cdot \mathbf{p}_i + (\beta_i - 1)c^2 - V_N(r_i)] + \sum_{i<j} \left[\frac{1}{r_{ij}} + g^{\text{B}}(r_{ij}) \right], \quad (2)$$

where α and β are the Dirac matrices, and the last two terms, $1/r_{ij}$ and $g^{\text{B}}(r_{ij})$, are the Coulomb and Breit interactions, respectively. In the FSRCC method, $|\Psi_{vw}\rangle$ can be written as

$$|\Psi_{vw}\rangle = e^T [1 + S_1 + S_2 + \frac{1}{2}(S_1^2 + S_2^2) + R] |\Phi_{vw}\rangle. \quad (3)$$

Here, $vw \dots$ represent the valence orbitals and $|\Phi_{vw}\rangle = a_w^\dagger a_v^\dagger |\Phi_0\rangle$ is the Dirac-Fock reference state for the two-valence atom or ion. And, T , S , and R are coupled-cluster (CC) operators for the closed-shell, one-valence, and two-valence sectors of the Hilbert space of the total electrons.

For a two-valence system with N electrons, T , S , and R operators in principle can have all possible excitations of the electrons, and therefore can be expressed as

$$T = \sum_{i=1}^{N-2} T_i, \quad S = \sum_{i=1}^{N-1} S_i, \quad \text{and} \quad R = \sum_{i=1}^N R_i. \quad (4)$$

However, among all the excitations, the single and double subsume most of the electron correlation effects. And, therefore, we can approximate $T = T_1 + T_2$, $S = S_1 + S_2$, and $R = R_2$, which is referred to as the coupled-cluster with singles and doubles (CCSD) approximation. The dominant contributions from the triple excitations are, however, also included in the present work using the perturbative triples approach, discussed later in the paper. In the second quantized notation, these operators can be represented as

$$T_1 = \sum_{ap} t_a^p a_p^\dagger a_a \quad \text{and} \quad T_2 = \frac{1}{2!} \sum_{abpq} t_{ab}^{pq} a_p^\dagger a_q^\dagger a_b a_a, \quad (5a)$$

$$S_1 = \sum_p s_v^p a_p^\dagger a_v \quad \text{and} \quad S_2 = \sum_{apq} s_{va}^{pq} a_p^\dagger a_q^\dagger a_a a_v, \quad (5b)$$

$$R_2 = \sum_{pq} r_{vw}^{pq} a_p^\dagger a_q^\dagger a_w a_v. \quad (5c)$$

Here, the indices $ab \dots$ and $pq \dots$ represent the core and virtual orbitals, respectively. And, t^{\dots} , s^{\dots} , and r^{\dots} are the cluster amplitudes corresponding to T , S , and R CC operators, respectively.

The closed-shell and one-valence CC operators are obtained by solving the set of coupled nonlinear equations discussed in our previous works (Refs. [15] and [21], respectively). Moreover, the details related to the computational implementation of the RCC method for closed-shell and one-valence systems is given in Ref. [22], where we had reported the details of our RCC codes. The two-valence CC operator R_2 is the solution of the equation [20]

$$\langle \Phi_{vw}^{pq} | \bar{H}_N + \{ \bar{H}_N S' \} + \{ \bar{H}_N R_2 \} | \Phi_{vw} \rangle = E_{vw}^{\text{att}} \langle \Phi_{vw}^{pq} | [S' + R_2] | \Phi_{vw} \rangle. \quad (6)$$

Here, for compact notation we have used $S' = S_1^{(1)} + S_2^{(1)} + \frac{1}{2}(S_1^{(1)2} + S_2^{(1)2})$. E_{vw}^{att} is the two-electron attachment energy and it is the difference between the correlated energy of the $(n-2)$ -electron (closed-shell) sector and the n -electron (two-valence) sector, $E_{vw} - E_0$. Alternatively, it can also be expressed as

$$E_{vw}^{\text{att}} = \epsilon_v + \epsilon_w + \Delta E_{vw}^{\text{att}}, \quad (7)$$

where ϵ_v and ϵ_w are the Dirac-Fock energies of the valence electrons in $|\phi_v\rangle$ and $|\phi_w\rangle$, respectively, and $\Delta E_{vw}^{\text{att}} = \Delta E_{vw}^{\text{corr}} - \Delta E_0^{\text{corr}}$ is the difference of the correlation energies of closed-shell and two-valence sectors.

III. PROPERTIES CALCULATION USING FSRCC

A. Hyperfine matrix elements

In this section we describe the properties calculation using the two-valence FSRCC method. For a detailed discussion we consider the matrix elements of the hyperfine interaction. The approach, however, is also applicable for calculation of properties associated with other one-body operators with appropriate selection rules. The hyperfine interaction is the coupling between the nuclear electromagnetic moments and the electromagnetic fields of the electrons. And the hyperfine interaction Hamiltonian [23] is

$$H_{\text{HFS}} = \sum_i \sum_{k,q} (-1)^q t_q^k(\hat{\mathbf{r}}_i) T_{-q}^k, \quad (8)$$

where $t_q^k(\mathbf{r})$ and T_q^k are the irreducible tensor operators of rank k in the electronic and nuclear sectors, respectively.

Using the two-valence RCC wave function from Eq. (3), the hyperfine matrix element in the electronic sector is

$$\langle \Psi_i | H_{\text{HFS}}^e | \Psi_j \rangle = \sum_{kl} c_k^{i*} c_l^j [\langle \Phi_k | \tilde{H}_{\text{HFS}}^e + \tilde{H}_{\text{HFS}}^e (S' + R_2) + (S' + R_2)^\dagger \tilde{H}_{\text{HFS}}^e + (S' + R_2)^\dagger \times \tilde{H}_{\text{HFS}}^e (S' + R_2) | \Phi_l \rangle], \quad (9)$$

where, H_{HFS}^e is the electronic component of the hyperfine operator. And, for compact notation, we represent the two-valence state $|\Psi_{vw}\rangle$ with $|\Psi_i\rangle$. The constants c_j^i are the mixing coefficients corresponding to the configuration state function $|\Phi_j\rangle$ for the state $|\Psi_i\rangle$, and are obtained by diagonalizing the effective Hamiltonian matrix [20] within the chosen model space. The dressed hyperfine Hamiltonian $\tilde{H}_{\text{HFS}}^e = e^{T^\dagger} H_{\text{HFS}}^e e^T$ is a nonterminating series of closed-shell CC operators T . In

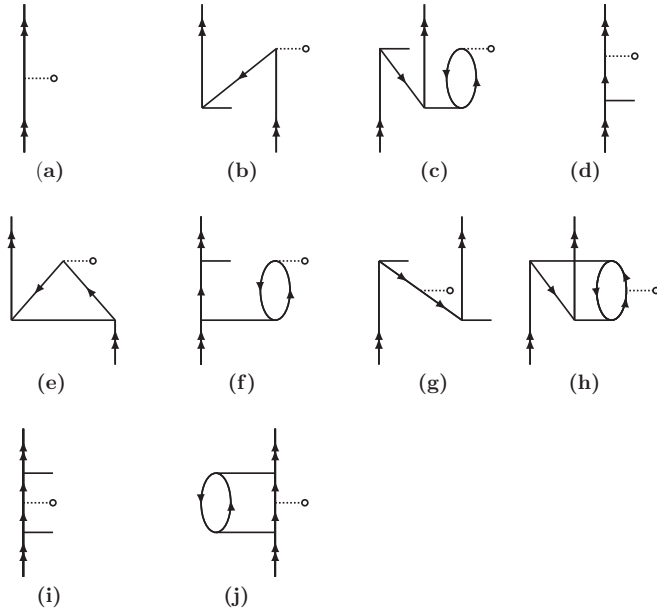


FIG. 1. (a) The DF diagram. [(b)–(j)] Some contributing example diagrams to Eq. (12). The diagrams are given in the same sequence as the terms in Eq. (12).

our previous work [21] we proposed an iterative scheme to include a class of dominant diagrams to all orders of T in \tilde{H}_{HFS}^e . And we also showed that the terms cubic in T and higher contribute less than 0.1% to the properties. So, in the present work, we truncate \tilde{H}_{HFS}^e to second order in T and include the terms $\tilde{H}_{\text{HFS}}^e \approx H_{\text{HFS}}^e + H_{\text{HFS}}^e T + T^\dagger H_{\text{HFS}}^e + T^\dagger H_{\text{HFS}}^e T$ in the properties calculations.

Next, to assess the contributions from different sectors we group the terms in Eq. (9) as

$$\langle \Psi_i | H_{\text{HFS}}^e | \Psi_j \rangle = \langle \Psi_i | H_{\text{HFS}}^e | \Psi_j \rangle_{\text{DF}} + \langle \Psi_i | H_{\text{HFS}}^e | \Psi_j \rangle_{1v} + \langle \Psi_i | H_{\text{HFS}}^e | \Psi_j \rangle_{2v}. \quad (10)$$

Here, the first, second, and third terms denote the contributions from the Dirac-Fock, one-valence, and two-valence sectors, respectively. The CC terms arising from each of the sectors are discussed in more detail.

1. Dirac-Fock contribution

The Dirac-Fock (DF) term is expected to have the dominant contribution among the three terms in Eq. (10). It is the expectation of the bare hyperfine Hamiltonian operator

$$\langle \Psi_i | H_{\text{HFS}}^e | \Psi_j \rangle_{\text{DF}} = \sum_{kl} c_k^{i*} c_l^j \langle \Phi_k | H_{\text{HFS}}^e | \Phi_l \rangle. \quad (11)$$

In terms of Goldstone diagrams, it has only one diagram and it is shown in Fig. 1(a). Since H_{HFS}^e is a one-body operator, the contribution is the expectation of H_{HFS}^e with respect to a valence orbital and then coupled with a spectator valence orbital. The angular momentum diagram from the coupling is topologically equivalent to the one in Fig. 2 with the effective operator $H_{\text{HFS}}^{\text{eff},k}$ replaced by H_{HFS}^k . The labels $j_v, j_w, \dots (J_i, J_j)$ denote the angular momentum quantum numbers of uncoupled (coupled) states, and multipole k represents the rank of the hyperfine operator.

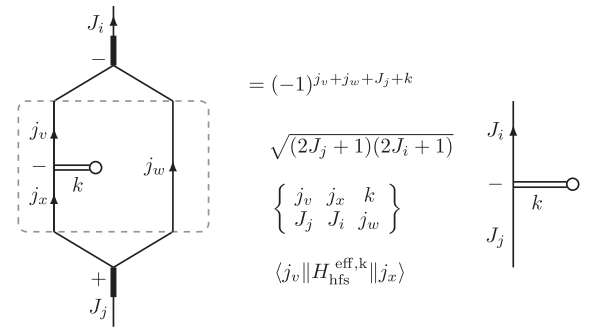


FIG. 2. Angular factor arising from the coupling of the one-body effective operator and a spectator valence line. The free diagram on the right-hand side represents the geometrical part in the Wigner-Eckart theorem.

2. $\langle \Psi_i | H_{\text{HFS}}^e | \Psi_j \rangle_{1v}$ contribution

The contribution in this sector involves both the T and S operators. From Eq. (9) we can write

$$\begin{aligned} \langle \Psi_i | H_{\text{HFS}}^e | \Psi_j \rangle_{1v} = & \sum_{kl} c_k^{i*} c_l^j [\langle \Phi_k | (H_{\text{HFS}}^e T_1 + T_1^\dagger H_{\text{HFS}}^e T_2 \\ & + \tilde{H}_{\text{HFS}}^e S_1 + \tilde{H}_{\text{HFS}}^e S_2 + S_1^\dagger \tilde{H}_{\text{HFS}}^e S_2) + \text{H.c.} \\ & + T_1^\dagger H_{\text{HFS}}^e T_1 + T_2^\dagger H_{\text{HFS}}^e T_2 + S_1^\dagger \tilde{H}_{\text{HFS}}^e S_1 \\ & + S_2^\dagger \tilde{H}_{\text{HFS}}^e S_2 | \Phi_l \rangle]. \end{aligned} \quad (12)$$

The above terms lead to 64 Goldstone diagrams and example diagrams are shown Figs. 1(b)–1(j). The leading-order contribution is expected from $\tilde{H}_{\text{HFS}}^e S$ and its Hermitian conjugate $S^\dagger \tilde{H}_{\text{HFS}}^e$. The example diagrams of $\tilde{H}_{\text{HFS}}^e S$ are shown in Figs. 1(d) and 1(e). The next-leading-order contribution is expected to be from the terms with two orders of S operators, $S^\dagger \tilde{H}_{\text{HFS}}^e S$. The example diagrams corresponding to this term are shown in Figs. 1(f), 1(i), and 1(j). To compute the contribution from $\langle \Psi_i | H_{\text{HFS}}^e | \Psi_j \rangle_{1v}$, first we compute the matrix elements with respect to uncoupled states and store them in the form of a one-body effective operator. And then, like in the DF approach, this effective operator is coupled with a spectator valence state.

3. $\langle \Psi_i | H_{\text{HFS}}^e | \Psi_j \rangle_{2v}$ contribution

This term has contributions from all types of CC operators, T , S , and R :

$$\begin{aligned} \langle \Psi_i | H_{\text{HFS}}^e | \Psi_j \rangle_{2v} = & \sum_{kl} c_k^{i*} c_l^j [\langle \Phi_k | (T_1^\dagger H_{\text{HFS}}^e T_2 + \tilde{H}_{\text{HFS}}^e S_2 \\ & + \tilde{H}_{\text{HFS}}^e R_2 + S_1^\dagger \tilde{H}_{\text{HFS}}^e S_2 + (S_1 + S_2)^\dagger \\ & \times \tilde{H}_{\text{HFS}}^e R_2 + S_1^{2\dagger} \tilde{H}_{\text{HFS}}^e (S_2 + R_2)) \\ & + \text{H.c.} + T_2^\dagger H_{\text{HFS}}^e T_2 + S_2^\dagger \tilde{H}_{\text{HFS}}^e S_2 \\ & + R_2^\dagger \tilde{H}_{\text{HFS}}^e R_2 | \Phi_l \rangle]. \end{aligned} \quad (13)$$

Here, we have neglected the terms with more than two orders in S_2 as these will have negligible contribution. There are 68 diagrams which arise from this term. Like in the one-valence sector, we give selected diagrams from this term in Fig. 3 as an example. The leading-order contribution is expected to

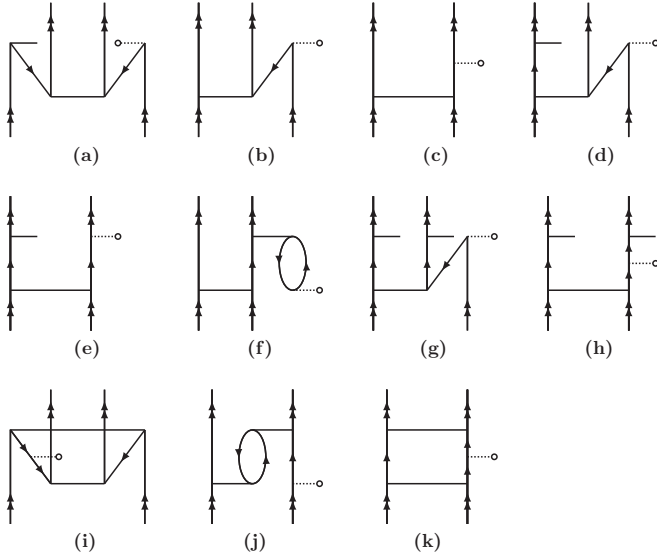


FIG. 3. Some contributing example diagrams to Eq. (13). For easy identification, diagrams are given in the same sequence as the terms in Eq. (13).

be $\tilde{H}_{\text{HFS}}^e R_2$ and its Hermitian conjugate $R_2^\dagger \tilde{H}_{\text{HFS}}^e$. The corresponding example diagram from these terms is shown in Fig. 3(c). This is on account of two important reasons. First, these are the lowest-order terms in R_2 . Second, the magnitude of R_2 is larger than the T and S . The next-leading-order contribution is expected to be $\tilde{H}_{\text{HFS}}^e S_2$ and its Hermitian conjugate as these are one order in S . The corresponding example diagram is shown in Fig. 3(b). Among the terms which are second or higher order in CC operators, the dominant contribution is expected from the term $R_2^\dagger \tilde{H}_{\text{HFS}}^e R_2$. Diagrammatically, an example is shown in Fig. 3(k). The reason for this is attributed to the larger magnitudes of R_2 operators. The remaining terms are expected to have negligible contributions. To compute the contribution from $\langle \Psi_i | H_{\text{HFS}}^e | \Psi_i \rangle_{2v}$, all the terms in Eq. (13) are computed with respect to uncoupled states first and then stored in the form of a two-body effective operator, as shown in Fig. 4. And, as indicated in the figure, the angular momenta of the valence electrons are coupled.

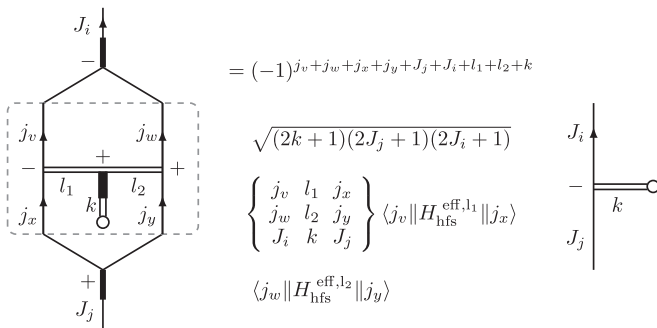


FIG. 4. Angular factor arising from the coupling of two-body effective operator. The portion in the dashed rectangle is an effective operator which subsumes the contribution from Eq. (13) in terms of uncoupled states.

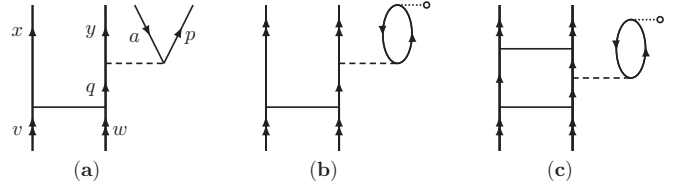


FIG. 5. (a) The perturbative R_3 diagram. [(b),(c)] The hyperfine matrix element diagrams from the terms $H_{\text{HFS}}^e R_3$ and $R_2^\dagger H_{\text{HFS}}^e R_3$. The dashed line represents the two-body residual interaction, g_{ij} , between the electrons.

B. Contribution from perturbative R_3

To account for the electron correlation effects from triple excitations, we consider the perturbative triples. With this approach we can incorporate the dominant contributions from triple excitations, but with far less computational cost than the full triples. For this, we choose the triples which arise from the two-valence CC operator R_2 , and the term is $\overline{g}R_2$, where $g_{ij} = \sum_{i<j} [\frac{1}{r_{ij}} + g^B(r_{ij})]$, the two-body residual interaction. This has the leading-order contribution to triples, since the magnitude of R_2 is larger than T and S for two-valence systems. The diagram corresponding to $\overline{g}R_2$ is shown in Fig. 5(a), and the algebraic expression is

$$R_3 \approx \frac{1}{\Delta \epsilon_{vwa}^{xyp}} a_x^\dagger a_y^\dagger a_p^\dagger a_a a_w a_v \sum_q \langle y p | g | q a \rangle \langle x q | R_2 | v w \rangle, \quad (14)$$

where $\Delta \epsilon_{vwa}^{xyp} = \epsilon_v + \epsilon_w + \epsilon_a - \epsilon_x - \epsilon_y - \epsilon_p$. The operator R_3 contracts with other CC operators along with the hyperfine operator and contributes to the properties through Eq. (9). In our previous work on two-valence systems [20], the dominant contribution to the properties involved the cluster operator R_2 . So, in the present work, to account for the contribution from R_3 we include the terms $H_{\text{HFS}}^e R_3$, $R_3^\dagger H_{\text{HFS}}^e$, $R_2^\dagger H_{\text{HFS}}^e R_3$, and $R_3^\dagger H_{\text{HFS}}^e R_2$. There are three diagrams from each of these terms which contribute to the two-valence properties. And, as an example, one diagram each from the terms $H_{\text{HFS}}^e R_3$ and $R_2^\dagger H_{\text{HFS}}^e R_3$ are shown in Figs. 5(b) and 5(c), respectively.

C. Hyperfine-induced $E1$ transition

The hyperfine eigenstate $|\Gamma F M_F\rangle$ is obtained by coupling the electronic state $|\Psi_{vw}\rangle$ with the eigenstate of the nuclear spin I . Considering the hyperfine interaction H_{HFS} as a perturbation and using the first-order time-independent perturbation theory,

$$|\Gamma F M_F\rangle = \sum_n \left[\frac{\langle \gamma_n J_n \gamma_l I | H_{\text{HFS}} | \gamma_0 J_0 \gamma_l I \rangle}{E_{J_0} - E_{J_n}} \right] \times |\gamma_n J_n \gamma_l I\rangle. \quad (15)$$

The term within the brackets represents the hyperfine mixing of the unperturbed state $|\gamma_0 J_0 \gamma_l I\rangle$ with an excited state $|\gamma_n J_n \gamma_l I\rangle$. The parameters Γ and γ_i are additional quantum numbers to identify the states uniquely, and E_J is the exact energy. The transition amplitude between two hyperfine states $|\Gamma_i F_i M_{F_i}\rangle$ and $|\Gamma_j F_j M_{F_j}\rangle$ is

$$E1_{\text{HFS}} = \langle \Gamma_i F_i M_{F_i} | \mathbf{D} | \Gamma_j F_j M_{F_j} \rangle, \quad (16)$$

where \mathbf{D} is the electric dipole operator. Using the expression for $|\Gamma F M_F\rangle$ from Eq. (15) in the above equation, we obtain the expression for the E_{HFS} -induced $^1S_0 \rightarrow ^3P_0^o$ transition amplitude as

$$E_{\text{HFS}} = c(I, J, F, \mu_I) \left[\frac{\langle ^1S_0 || d || ^3P_1^o \rangle \langle ^3P_1^o || t^1 || ^3P_0^o \rangle}{\Delta E_{^3P_1^o}} + \frac{\langle ^1S_0 || d || ^1P_1^o \rangle \langle ^1P_1^o || t^1 || ^3P_0^o \rangle}{\Delta E_{^1P_1^o}} \right], \quad (17)$$

where $c(I, J, F, \mu_I)$ is the angular factor associated with the hyperfine wave function in Eq. (15), and $\Delta E_{^3P_1^o}$ and $\Delta E_{^1P_1^o}$ are the energy differences $E_{^3P_0^o} - E_{^3P_1^o}$ and $E_{^3P_0^o} - E_{^1P_1^o}$.

IV. RESULTS AND DISCUSSIONS

A. Convergence of basis

To obtain accurate results it is crucial to use a basis set which provides a good description of the single-electron wave functions and energies. And, to incorporate the effects of finite charge distribution of the nucleus we use a two-parameter finite-size Fermi density distribution. In this work, we use the Gaussian-type orbitals (GTOs) [24] as the single-electron basis. The orbital as well as the self-consistent-field energies are optimized to match the GRASP2K [25] data. We achieve an excellent match and details of the comparison are reported in our recent work [17]. The orbital basis used in the present work also incorporates the effects of Breit interaction, vacuum polarization, and the self-energy corrections. For Breit interaction, we employ the expression given in Ref. [26] and incorporate it in the orbital generation as well as the FSRCC calculations. The effect of vacuum polarization on single-electron orbitals is considered using the Uehling potential [27] modified for the finite-size nucleus [28]. The self-energy corrections to the orbitals are incorporated through the model Lamb-shift operator introduced by Shabaev *et al.* [29], and are calculated using the code QEDMOD [30].

Mathematically, the GTO bases are incomplete [31] and, hence, it is essential to check the convergence of results with basis size. For this, we start with a moderate basis of 86 orbitals ($14s, 14p, 9d, 5f, 4g, 4h$) and add orbitals in each symmetry until the change in the properties is $\leq 10^{-3}$ in respective units of the properties. For illustrative purposes the convergence trend of the magnetic dipole hyperfine structure (HFS) constant is shown in Fig. 6(a). It is observed that the change is less than 10^{-3} MHz when the basis is augmented from 167 to 173. So, to optimize the computational time, we consider the basis set with 167 ($23s, 23p, 15d, 12f, 11g, 11h$) orbitals as optimal, and use it in the properties computations.

B. Excitation energies

In Table I, we list the low-lying energies of Al^+ from our results along with other theory and experimental data for comparison. From the table it is evident that our results are in good agreement with experimental as well as previous theoretical results. The largest and smallest relative errors in our calculation are 0.9% and 0.004%, in the case of $3p^2 \ ^3P_2$ and $3s3p \ ^3P_0^o$ states, respectively. It is to be

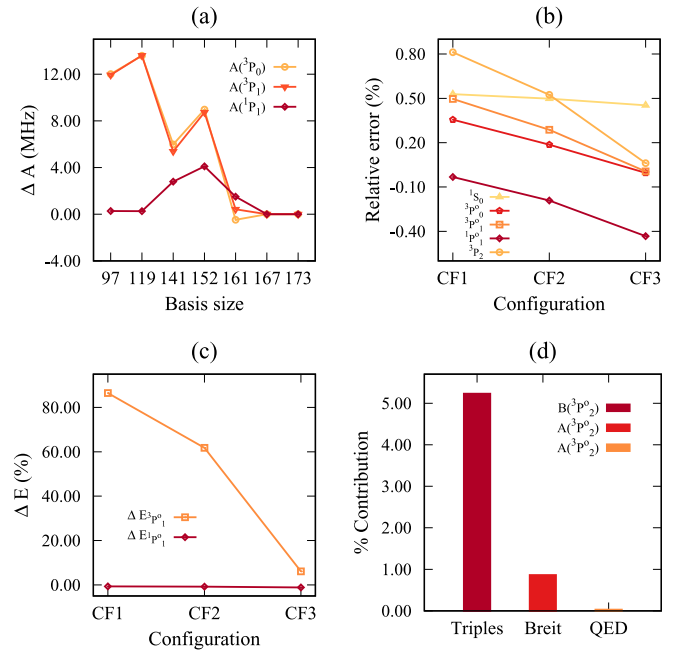


FIG. 6. The convergence trend of HFS constants as a function of (a) basis size and of relative errors in (b) the excitation energy and (c) the energy separation as a function of configurations, and maximum percentage contributions from the perturbative triples, Breit interaction, and QED corrections to HFS constants.

noted that the states with low energy configurations $3s^2$ and $3s3p$, which are key to clock transition, are very close to the experiment. Among the previous theoretical results, those from the configuration-interaction+all-order (CI+AO) calculations by Konovalova and collaborators [33] and Safronova and collaborators [11] are in better agreement with the experimental data. The maximum relative error is $\approx 0.14\%$ in each of these calculations, in the case of $3s3d \ ^3D_2$ and $3s3p \ ^1P_1^o$ states, respectively. The reason for the marginal difference between these calculations and ours can be attributed to the different treatment of *core-core* and *core-valence* correlations. In Refs. [33] and [11], a linearized CCSD is used in the calculation. However, in the present work, we include the nonlinear terms in the CCSD. Hence, our work considers the electron correlation effects better than the previous works. This naturally translates to improved overall uncertainty. The other set of reliable results, in terms of proximity to the experimental data, is based on the configuration-interaction with a semi-empirical core potential (CICP) method obtained by Mitroy and collaborators [34]. The remaining theoretical results are either based on many-body perturbation theory or multiconfiguration Dirac-Hartree-Fock (MCDHF) and these have larger deviations from the experiment. Considering the contributions from the Breit and QED corrections, we observe the largest combined contribution of $\approx 0.01\%$ of the total value in the case of $^3P_0^o$. The magnitude is consistent with the previous calculation [33].

To discern the electron correlation effects, the energies are computed with three different model spaces. We start with the configurations $3s^2 + 3s3p$ (CF1) in the model space and then add $3s4s$ and $3p^2 + 3s3d$ in the two subsequent computations,

TABLE I. Energy (in cm^{-1}) of the ground state $3s^2\ ^1S_0$ and the excitation energies of low-lying excited states using the configurations $3s^2 + 3s3p + 3p^2 + 3s3d + 3s4s$ in the model space. Listed energies also incorporate the contributions from the Breit interaction and QED corrections, and are obtained using the converged basis of 167 orbitals.

States	FSRCC	Other calculations	Expt. [32]
$3s^2\ ^1S_0$	379582	381210, ^a 381331, ^b 381287 ^c 382024 ^d	381308
$3s3p\ ^3P_0^o$	37395	37392, ^a 37374, ^c 37396 ^b 37191 ^d	37393
$3s3p\ ^3P_1^o$	37452	36705, ^e 35000, ^f 37454 ^a 36292, ^g 37516, ^h 37457 ^b 37818, ⁱ 37253, ^j 37251 ^d	37454
$3s3p\ ^3P_2^o$	37555	37579, ^a 37572, ^b 37374 ^d	37578
$3s3p\ ^1P_1^o$	60111	60723, ^c 63000, ^f 59855 ^a 59849, ^c 59427, ^g 60198 ^b 59768, ^b 59140, ⁱ 60104 ^j 54410 ^d	59852
$3p^2\ ^1D_2$	85578	85450, ^a 85462, ^b 85678 ^d	85481
$3s4s\ ^3S_1$	91043	91256, ^a 91289, ^b 91262 ^c	91274
$3p^2\ ^3P_0$	93379	94049, ^a 94092, ^b 93672 ^d	94085
$3p^2\ ^3P_1$	93380	94112, ^a 94151, ^b 93735 ^d	94147
$3p^2\ ^3P_2$	93409	94234, ^a 94265, ^b 93857 ^d	94269
$3s4s\ ^1S_0$	95156	95336, ^a 95354 ^b	95350.60
$3s3d\ ^3D_1$	95248	95420, ^a 95527, ^b 95532 ^c 95695 ^d	95551
$3s3d\ ^3D_2$	95252	95419, ^a 95527, ^b 95697 ^d	95550
$3s3d\ ^3D_3$	95253	95418, ^a 95524, ^b 95690 ^d	95549
$3s3d\ ^1D_2$	110382	106270 ^d	110090
$3p^2\ ^1S_0$	111598		111637

^aReference [33] (CI+AO).

^bReference [11] (CI+AO).

^cReference [34] (CICP).

^dReference [41] Relativistic many-body perturbation theory (RMBPT).

^eReference [35] Configuration interaction Dirac-Fock with core polarization.

^fReference [36] (MCDF).

^gReference [37] Multiconfiguration relativistic random-phase approximation (MCRRPA).

^hReference [38] (MCDHF).

ⁱReference [39] (RMBPT).

^jReference [40] (MCDF).

CF2 and CF3, respectively. We could not separate the contribution from $3p^2$ and $3s3d$ as the inclusion of any one of these leads to divergence due to the *intruder* states. To elaborate, when only $3p^2$ is included in the model space, $3s3d\ ^3D_{1,2,3}$ states, having energies within the range of the model space, are the intruder states. This leads to divergence due to a small energy denominator. Similarly, when only $3s3d$ is included, $3p^2\ ^3P_{0,1,2}$ states are intruder states. The trends of the results from the three model spaces are shown in Figs. 6(b) and 6(c). The plots in the figures show that the inclusion of $3p^2$, $3s3d$, and $3s4s$ in the model space improves the energies of the $3s^2\ ^1S_0$ and $3s3p\ ^3P_{0,1,2}^o$ states, and the energy difference $\Delta E_{3p_0^o} = E_{3p_0^o} - E_{3p_1^o}$. Obtaining correct values for the energy difference $\Delta E_{3p_0^o}$ is the key to obtain the accurate lifetime of

the $^3P_0^o$ state. The improvement can be attributed to the inclusion of *valence-valence* correlation effects more accurately by diagonalizing the effective Hamiltonian in a larger model space. As a result, $\Delta E_{3p_0^o}$ increases from 8.24 to 57.76 cm^{-1} , which is in good agreement with the experimental result of 60.88 cm^{-1} . This improves the lifetime of the $^3P_0^o$ state by about 96%. We, however, observe an opposite trend for the excitation energy of the $^1P_1^o$ state and, hence, the value of the energy difference $\Delta E_{1p_1^o}$ as well. But these have a negligible effect on the lifetime of $^3P_0^o$ as $\Delta E_{1p_1^o}$ is very large, $\approx 22457\ \text{cm}^{-1}$. It must be emphasized that the two-valence coupled-cluster calculations with larger model space are challenging. And our present work demonstrates the possibility of doing this with the FSRCC method without ambiguity by augmenting the model space systematically.

C. Hyperfine and dipole reduced matrix elements and structure constants

The magnetic dipole and electric quadrupole hyperfine constants, A and B , respectively, obtained from our study are listed in the Table II. In addition, the off-diagonal reduced matrix elements required to evaluate the $E1_{\text{HFS}}$ amplitude are presented in Table III. For quantitative assessment the contributions from the Breit interactions, QED corrections, and dominant triples are also listed in the table. For all the states CCSD is the dominant contribution. And the DF term has the leading-order contribution among the different sectors in the CCSD: it accounts for more than 90% of the total value. More importantly, within 2ν , $H_{\text{HFS}}^e R_2 + \text{H.c.}$ has the largest contribution. This can be attributed to the larger magnitude of the R_2 operator. As discernible from Fig. 6(d), the contribution from the perturbative triples R_3 is also crucial. For example, it has $\approx 3\%$ and 5% of the total value of $A(^1P_1^o)$ and $B(^3P_2^o)$, respectively. This implies that the triples must be included in the FSRCC calculations to obtain accurate results for hyperfine structure and related properties of Al^+ . From the Breit interaction, $A(^3P_2^o)$ has the largest contribution, $\approx 0.9\%$. Considering the level of accuracy needed for clock properties, it is a significant contribution and cannot be neglected. The contribution from the QED corrections is $\approx 0.02\%$ and negligible compared to the other terms.

To the best of our knowledge, there are no experimental data for comparison. However, there is one theoretical result each for A and B of $^3P_1^o$ and $^3P_2^o$ using the MCDF method by Itano and collaborators [42]. Our results of 1389.81, 1174.29, and 16.65 for $A(^3P_1^o)$, $A(^3P_2^o)$, and $B(^3P_1^o)$, respectively, are $\approx 3.1\%$, 2.2% , and 5.6% larger than the values given in Ref. [42]. The reason for this difference can be attributed to the better accounting of the electron correlations in FSRCC theory as it includes the residual Coulomb interaction to all orders. We observe an opposite trend for $B(^3P_2^o)$. Our DF result, 29.44, is close to the MCDF result, 31.42 [42], but our total value of 24.23 is 45.7% lower. This is due to the large cancellation from the 2ν sector. For the off-diagonal reduced matrix elements, there are two previous results for comparison. The magnitudes of the reduced matrix elements t_{30} and t_{10} from our calculation are smaller than the MCDHF [13] and CI + MBPT [43] results. The reason for this can be attributed to the difference in the treatment of the electron

TABLE II. Magnetic dipole and electric quadrupole hyperfine structure constants (in MHz) for $^3P_1^o$, $^3P_2^o$, and $^1P_1^o$ states. The values of the nuclear magnetic dipole moment $\mu_I = 3.6415069(7)\mu_N$ and electric quadrupole moment $Q = 0.1466(10)$ b are used in the calculation.

Methods	Hyperfine structure constants					
	A			B		
	$^3P_1^o$	$^3P_2^o$	$^1P_1^o$	$^3P_1^o$	$^3P_2^o$	$^1P_1^o$
CCSD	1385.409	1188.024	292.588	-16.173	25.549	27.876
CCSD(T)	8.316	-3.865	-8.661	-0.473	-1.276	0.432
Breit	-4.240	-10.194	2.153	-1.633×10^{-4}	1.246×10^{-3}	-2.745×10^{-4}
Vacuum polarization	0.306	0.306	-4.118×10^{-4}	4.069×10^{-5}	-3.715×10^{-5}	-1.956×10^{-4}
Self-energy	0.023	0.023	3.790×10^{-4}	2.561×10^{-6}	4.323×10^{-5}	3.966×10^{-5}
Total	1389.814	1174.294	286.0800	-16.646	24.274	28.308
Other calculations	1348 ^a	1149 ^a		-15.62 ^a	31.42 ^a	

^aReference [42] (MCDHF).

correlations in FSRCC and these calculations. For the results in Ref. [13], there could be two sources of uncertainty in the matrix elements. First, the active space of configuration state functions (CSFs) is limited to the single-electron basis with $n = 7$ and $l = 5$ only, where n and l are principal and orbital quantum numbers, respectively. And second, the core polarization effect is considered only from the $2s$ and $2p$ electrons. In the present work, however, we include a large active space with orbitals up to $n = 25$ and $l = 6$, and CSFs arising from all core-to-valence, valence-to-virtuals and core-to-virtuals single and double electron replacements. In addition, we also include the contribution from triple excitations perturbatively. Coming to the results in Ref. [43], there is an important difference in terms of accounting of the *core-core* and *core-valence* correlations. In the present work, these are considered up to all orders of residual Coulomb interaction. Reference [43], however, considers these up to third order only. It is to be also mentioned that the uncertainty in the reduced matrix elements in Ref. [43] is 3%.

We use the $E1$ transition reduced matrix elements in Table III to compute the oscillator strengths, which are listed in Table IV. Like hyperfine structure constants, the dominant contribution is from the CCSD. It contributes more than 94% of the total value. The contributions from the perturbative triples and Breit interactions are significant. The maximum contributions from these are $\approx 6.2\%$ and 0.4% , respectively. Like the hyperfine case, QED correction has a negligible

contribution. For the oscillator strength of the $^1S_0 \rightarrow ^3P_1^o$ transition there is one experimental result and it is based on the time-resolved technique [44]. Our theoretical result, 2.60×10^{-5} a.u., for this transition has the same order of magnitude as the experimental data, $(1.068 \pm 0.074) \times 10^{-5}$ a.u., but it is $\approx 128\%$ larger. The other theoretical results, although based on MCDF or related methods, show wide variation. The results range from 0.36×10^{-5} [36] to 3.78×10^{-5} a.u. [35]. For the $^1S_0 \rightarrow ^1P_1^o$ transition there are three experimental results based on the beam-foil technique [45–47]. Despite the same experimental technique, there is a large variation in the results. In addition, the uncertainties associated with the results are large; these are in the range $\approx 4.8\%$ [46] to 15.8% [45,47]. Our theoretical result of 1.47 lies within the range of the experimental values. One observation is that the previous theoretical results are similar in values. The reason for this could be the similar treatment of the electron correlations as all are based on MCDF and its variations and have similar shortcomings in the inclusion of electron-correlation effects. This highlights the importance of cross-checking with other methods like we have done with a better method.

D. $E1_{\text{HFS}}$

Using the electric dipole and hyperfine reduced matrix elements from Table III and the energy differences $\Delta E_{3P_1^o/1P_1^o}$ from Table I in Eq. (17), we calculate the $E1_{\text{HFS}}$ amplitude

TABLE III. Magnetic dipole hyperfine and $E1$ transition reduced matrix elements, $t_{30} = \langle ^3P_1^o || t^1 || ^3P_0^o \rangle$ and $t_{10} = \langle ^1P_1^o || t^1 || ^3P_0^o \rangle$, $d_{03} = \langle ^1S_0 || d || ^3P_1^o \rangle$ and $d_{01} = \langle ^1S_0 || d || ^1P_1^o \rangle$, in atomic units.

Methods	d_{03}	d_{01}	t_{30}	t_{10}
CCSD	-1.425×10^{-2}	2.841	-0.095	0.079
CCSD(T)	-9.384×10^{-4}	-9.159×10^{-4}	1.608×10^{-3}	-5.667×10^{-4}
Breit	6.303×10^{-5}	-2.069×10^{-5}	4.882×10^{-5}	-3.165×10^{-4}
Vacuum polarization	-9.737×10^{-7}	1.181×10^{-5}	-4.198×10^{-5}	3.035×10^{-5}
Self-energy	2.332×10^{-7}	5.608×10^{-7}	-2.993×10^{-6}	2.849×10^{-6}
Total	-1.513×10^{-2}	2.840	-0.094	0.078
Other calculations			-0.120 ^a	0.096 ^a
			-0.119 ^b	

^aReference [13] (MCDHF).

^bReference [43] (CI+MBPT).

TABLE IV. Oscillator strengths of the allowed transitions compared with other calculations and experiments.

Method	$^1S_0 \rightarrow ^3P_1^o$	$^1S_0 \rightarrow ^1P_1^o$
CCSD(T)+ Breit+QED	2.604×10^{-5}	1.473
Other calculations	3.560×10^{-6} , ^a 8.875×10^{-6} , ^b 3.776×10^{-5} , ^d 1.017×10^{-5} ^e	1.740, ^a 1.765, ^c 1.831, ^b 1.850, ^f 1.746, ^g 1.751, ^h 1.76, ^d 1.775 ^e
Experiments	$(1.068 \pm 0.074) \times 10^{-5i}$	1.74 ± 0.27 , ^j 1.9 ± 0.3 , ^k 1.26 ± 0.06 ^l

^aReference [36] (MCDF).^bReference [34] (CICP).^cReference [37] (MCRRPA).^dReference [35] (MCDF+CP).^eReference [13] (MCDHF).^fReference [48] (RRPA).^gReference [38] (MCDHF).^hReference [40] (MCDF).ⁱReference [44] (experiment).^jReference [45] (experiment).^kReference [47] (experiment).^lReference [46] (experiment).

of the $^1S_0 \rightarrow ^3P_0^o$ transition and the lifetime of the $^3P_0^o$ clock state. The results from the present and previous works are listed in Table V. The experimental value of the lifetime is 20.6 ± 1.4 s from Ref. [5]. This is in very good agreement with our theoretical value of 20.20 ± 0.91 s, identified as CCSD(T) + Breit + QED in the table. Here, one point is to be noted: the error associated with the experimental value, $\approx 6.8\%$, is not negligible. As discernible from the table, the contribution from the perturbative triples to the lifetime is $\approx -6.4\%$ of the total value and is essential to improve the comparison with the experimental result. The combined contribution from the Breit interaction and QED corrections is $\approx 0.8\%$ of the total value. Considering the current uncertainties of optical atomic clocks, this cannot be neglected to obtain theoretical results with commensurate uncertainties. Two previous theoretical works, using the MCDF method, have reported the lifetime of the $^3P_0^o$ state [12,13]. Between the two, the recent work of Ref. [13] treats the electron correlation more accurately by considering *single* and *double* electron replacements and larger active space for CSFs. However, the result of 23.11 s in Ref. [13] has a larger deviation ($\approx 12\%$) from the experimental data. This indicates inherent

shortcomings or inconsistencies of accounting for the electron correlation properly in the MCDF method. This is resolved in the present work. In the FSRCC method such inconsistencies do not arise. As mentioned earlier, we use a converged basis as the active space in which all possible *single* and *double* electron replacements are included to all orders.

V. THEORETICAL UNCERTAINTY

The theoretical uncertainty in the lifetime of the $^3P_0^o$ state depends on the uncertainties in the HFS reduced matrix elements t_{30} and t_{10} , the dipole reduced matrix elements d_{03} and d_{01} , and the energy denominators $\Delta E_{3P_1^o}$ and $\Delta E_{1P_1^o}$. For the reduced matrix elements, we have identified four sources which contribute to the theoretical uncertainty. The first source is the truncation of the basis set. As shown in Fig. 6(a) for the HFS constant, the change in the HFS and electric dipole matrix elements is of the order of 10^{-3} or less on augmenting the converged basis. Since the change is very small, we can neglect this uncertainty. The second source is the truncation of the dressed Hamiltonian \tilde{H}_{HFS}^c to second order in $T^{(0)}$. In our previous work on hyperfine structure constants [21], using an iterative scheme, we have shown that the contribution from third- and higher-order terms is less than 0.1%. So, we take 0.1% as an upper bound from this source of uncertainty. The third source is the partial inclusion of triple excitations in the properties calculation. Since we consider the leading-order terms of triple excitation in the perturbative triples, the contribution from the remaining terms will be small. Based on our analysis in present and previous works [17,49], we estimate the upper bound from this source as 0.72%. The fourth source of uncertainty is associated with the frequency-dependent Breit interaction, which is not included in the present work. However, in our previous work [50] using a series of computations with GRASP2K which implements this interaction we estimated an upper bound on this uncertainty to be 0.13% in Ra. Although Al^+ is a much lighter atom

TABLE V. Wavelength (λ) (in nm), $E1_{\text{HFS}}$ amplitude (in a.u.) of the $^1S_0 \rightarrow ^3P_0^o$ transition, and the lifetime (τ) (in seconds) of the $^3P_0^o$ metastable state.

Methods	λ	$E1_{\text{HFS}}$	τ
CCSD	267.44	5.153×10^{-5}	21.33
CCSD(T)		5.316×10^{-5}	20.04
CCSD(T)+Breit+QED		5.295×10^{-5}	20.20 ± 0.91
Other calculations			23.11 , ^a 20.33 ^b
Experiments	267.43		20.6 ± 1.4 ^c

^aReference [13] (MCDF).^bReference [12] (MCDF).^cReference [5] (experiment).

TABLE VI. Convergence of excitation energy, hyperfine structure constants, and electric dipole transition amplitudes as a function of basis size.

States or property	Basis size							
	BS1 ^a	BS2 ^b	BS3 ^c	BS4 ^d	BS5 ^e	BS6 ^f	BS7 ^g	BS8 ^h
Excitation energy								
$3s3p\ ^3P_0^o$	36880.92	36887.02	36893.38	37050.55	37388.70	37391.43	37391.43	37391.43
$3s3p\ ^3P_1^o$	36941.51	36947.51	36953.75	37109.51	37448.96	37449.19	37449.19	37449.19
$3s3p\ ^3P_2^o$	37050.77	37056.56	37062.55	37215.38	37557.29	37552.51	37552.52	37552.52
$3s3p\ ^1P_1^o$	60174.87	60177.54	60181.35	60186.27	60205.24	60109.38	60109.38	60109.38
$3p^2\ ^1D_2$	84935.91	84943.85	84951.80	85142.41	85605.12	85574.35	85574.35	85574.35
$3s4s\ ^3S_1$	90488.94	90494.85	90500.30	90670.08	91019.53	91041.40	91041.40	91041.40
$3p^2\ ^3P_0$	92789.16	92801.94	92816.68	92977.64	93367.32	93374.60	93374.59	93374.59
$3p^2\ ^3P_1$	92798.39	92810.12	92823.73	92986.81	93380.10	93375.69	93375.69	93375.69
$3p^2\ ^3P_2$	92882.82	92894.07	92907.51	93053.81	93411.63	93405.18	93405.18	93405.18
$3s4s\ ^1S_0$	94524.80	94531.58	94537.68	94717.64	95132.51	95154.58	95154.59	95154.58
$3s3d\ ^3D_1$	94950.56	94948.62	94943.20	95034.90	95321.19	95246.39	95246.39	95246.39
$3s3d\ ^3D_2$	94954.45	94952.51	94947.56	95039.24	95325.07	95250.27	95250.27	95250.27
$3s3d\ ^3D_3$	94957.27	94955.31	94950.02	95041.37	95326.47	95251.68	95251.68	95251.68
$3s3d\ ^1D_2$	109929.38	109931.55	109931.47	110085.40	110457.19	110379.43	110379.43	110379.43
$3p^2\ ^1S_0$	111441.00	111448.22	111453.87	111532.23	111733.69	111593.71	111593.71	111593.71
HFS constants								
$A(^3P_1^o)$	1345.337	1357.349	1370.930	1376.918	1385.889	1385.409	1385.410	1385.410
$A(^3P_2^o)$	1147.931	1159.867	1173.480	1178.863	1187.596	1188.024	1188.025	1188.025
$A(^1P_1^o)$	283.646	283.920	284.187	286.985	291.088	292.588	292.588	292.588
$B(^3P_1^o)$	-15.969	-15.978	-15.980	-16.059	-16.165	-16.173	-16.173	-16.173
$B(^3P_2^o)$	25.026	25.041	25.045	25.231	25.503	25.549	25.549	25.549
$B(^1P_1^o)$	27.340	27.355	27.358	27.576	27.825	27.876	27.876	27.876
$E1$ amplitude								
$^1S_0 \rightarrow ^3P_1^o$	-1.843×10^{-2}	-1.832×10^{-2}	-1.820×10^{-2}	-1.718×10^{-2}	-1.531×10^{-2}	-1.425×10^{-2}	-1.425×10^{-2}	-1.425×10^{-2}
$^1S_0 \rightarrow ^1P_1^o$	2.894	2.893	2.893	2.875	2.845	2.841	2.841	2.841

^a86 (14s, 14p, 9d, 5f, 4g, 4h).^b97 (15s, 15p, 10d, 6f, 5g, 5h).^c119 (17s, 17p, 12d, 8f, 7g, 7h).^d141 (19s, 19p, 14d, 10f, 9g, 9h).^e152 (20s, 20p, 15d, 11f, 10g, 10h).^f161 (21s, 21p, 15d, 12f, 11g, 11h).^g167 (23s, 23p, 15d, 12f, 11g, 11h).^h173 (25s, 25p, 15d, 12f, 11g, 11h).

and is expected to have a much smaller contribution from the frequency-dependent Breit interaction, we take 0.13% as an upper bound from this source. There could be other sources of theoretical uncertainty, such as the higher-order coupled perturbation of vacuum polarization and self-energy terms, quadruply excited cluster operators, etc. But these, in general, have much lower contributions to the properties and their cumulative theoretical uncertainty could be below 0.1%. The theoretical uncertainty associated with energy denominators $\Delta E_{3P_1^o}$ and $\Delta E_{1P_1^o}$ is calculated from the relative errors in the excitation energies of $^3P_0^o$, $^3P_1^o$, and $^1P_1^o$ states. These are $\approx 0.01\%$ and 0.43% , respectively.

The other theoretical uncertainty which will contribute to the lifetime is the QED corrections at the level of $E1_{\text{HFS}}$ calculation. To estimate this uncertainty, we refer to Refs. [51,52]. In these works Shabaev and collaborators have implemented and computed the one-loop QED corrections to the parity-nonconserving transition amplitudes. Considering that the magnetic dipole HFS is like the matrix element of the parity-violating interaction Hamiltonian, the associated theoretical

uncertainty would be similar. Thus, based on these works we consider 0.3% as the upper bound from this source of uncertainty. It is, however, to be noted that the actual uncertainty would be smaller as Al^+ is a much lighter system compared to the Cs and Fr atoms studied in Refs. [51,52]. So, by combining the upper bounds of all the contributions, the theoretical uncertainty associated with the value of the lifetime of the $^3P_0^o$ state is 4.5%.

VI. CONCLUSIONS

In conclusion, we have developed an all-particle Fock-space relativistic coupled-cluster based method to calculate the properties of two-valence atomic systems. To account for the relativistic effects and QED corrections we use the Dirac-Coulomb-Breit Hamiltonian with the corrections from the Uehling potential and the self-energy. The effects of the triple excitations are incorporated using the perturbative triples. Using the method we have calculated the properties such as the excitation energies, hyperfine structure constants and reduced

matrix elements, oscillator strengths, and the lifetime of the $^3P_0^o$ metastable state in Al^+ , which is an important parameter for the $^1S_0 \rightarrow ^3P_0^o$ clock transition. Our results of the excitation energies and oscillator strengths agree well with the experimental data. Most importantly, our theoretical estimate of the lifetime of the $^3P_0^o$ state, 20.20 ± 0.91 s, is in excellent agreement with the experimental value, 20.60 ± 1.4 s, from Rosenband *et al.* [5]. From our studies we conclude that the contributions from the triple excitations and Breit + QED corrections are essential to obtain accurate clock properties in Al^+ . Based on error analysis, the upper bound on the theoretical uncertainty in the calculated lifetime of $^3P_0^o$ is 4.5%. The level of uncertainty in our results indicates that the FSRCC method we have developed has the potential to predict the structure and properties of two-valence atoms and ions with accuracies commensurate with the experiments.

ACKNOWLEDGMENTS

We would like to thank B. P. Das for useful suggestions on the manuscript. One of the authors, B.K.M., acknowledges the funding support from the SERB (ECR/2016/001454). The results presented in the paper are based on the computations using the High Performance Computing cluster, Padum, at the Indian Institute of Technology Delhi, New Delhi.

APPENDIX: CONVERGENCE TABLE OF THE PROPERTIES WITH BASIS SIZE

In Table VI, we provide the trend of the convergence of excitation energies, magnetic dipole and electric quadrupole hyperfine constants, and electric dipole transition amplitudes as a function of basis size. As it is evident from the table, all the properties converge to the order of 10^{-3} or less in the respective units of the properties.

-
- [1] S. G. Karshenboim and E. Peik, *Astrophysics, Clocks and Fundamental Constants*, Lecture Notes in Physics (Springer, New York, 2010).
- [2] M. S. Grewal, A. P. Andrews, and C. G. Bartone, *Global Navigation Satellite Systems, Inertial Navigation, and Integration* (Wiley, New York, 2013).
- [3] M. S. Safronova, D. Budker, D. DeMille, D. F. J. Kimball, A. Derevianko, and C. W. Clark, Search for new physics with atoms and molecules, *Rev. Mod. Phys.* **90**, 025008 (2018).
- [4] F. Riehle, P. Gill, F. Arias, and L. Robertsson, The CIPM list of recommended frequency standard values: Guidelines and procedures, *Metrologia* **55**, 188 (2018).
- [5] T. Rosenband, P. O. Schmidt, D. B. Hume, W. M. Itano, T. M. Fortier, J. E. Stalnaker, K. Kim, S. A. Diddams, J. C. J. Koelemeij, J. C. Bergquist, and D. J. Wineland, Observation of the $^1S_0 \rightarrow ^3P_0$ Clock Transition in $^{27}\text{Al}^+$, *Phys. Rev. Lett.* **98**, 220801 (2007).
- [6] C. W. Chou, D. B. Hume, J. C. J. Koelemeij, D. J. Wineland, and T. Rosenband, Frequency Comparison of Two High-Accuracy Al^+ Optical Clocks, *Phys. Rev. Lett.* **104**, 070802 (2010).
- [7] J.-S. Chen, S. M. Brewer, C. W. Chou, D. J. Wineland, D. R. Leibbrandt, and D. B. Hume, Sympathetic Ground State Cooling and Time-Dilation Shifts in an $^{27}\text{Al}^+$ Optical Clock, *Phys. Rev. Lett.* **118**, 053002 (2017).
- [8] S. M. Brewer, J.-S. Chen, A. M. Hankin, E. R. Clements, C. W. Chou, D. J. Wineland, D. B. Hume, and D. R. Leibbrandt, $^{27}\text{Al}^+$ Quantum-Logic Clock with a Systematic Uncertainty Below 10^{-18} , *Phys. Rev. Lett.* **123**, 033201 (2019).
- [9] S. M. Brewer, J.-S. Chen, K. Belay, A. M. Hankin, E. R. Clements, C. W. Chou, W. F. McGrew, X. Zhang, R. J. Fasano, D. Nicolodi, H. Leopardi, T. M. Fortier, S. A. Diddams, A. D. Ludlow, D. J. Wineland, D. R. Leibbrandt, and D. B. Hume, Measurements of $^{27}\text{Al}^+$ and $^{25}\text{Mg}^+$ magnetic constants for improved ion-clock accuracy, *Phys. Rev. A* **100**, 013409 (2019).
- [10] M. Kállay, H. S. Nataraj, B. K. Sahoo, B. P. Das, and L. Visscher, Relativistic general-order coupled-cluster method for high-precision calculations: Application to the Al^+ atomic clock, *Phys. Rev. A* **83**, 030503(R) (2011).
- [11] M. S. Safronova, M. G. Kozlov, and C. W. Clark, Precision Calculation of Blackbody Radiation Shifts for Optical Frequency Metrology, *Phys. Rev. Lett.* **107**, 143006 (2011).
- [12] T. Brage, P. G. Judge, A. Aboussaid, M. R. Godefroid, P. Jonsson, A. Ynnerman, C. F. Fischer, and D. S. Leckrone, Hyperfine induced transitions as diagnostics of isotopic composition and densities of low-density plasmas, *Astrophys. J.* **500**, 507 (1998).
- [13] H. Kang, J. Li, C. Dong, P. Jonsson, and G. Gaigalas, Hyperfine quenching of the $3s3p^3P_0$ level in Mg-like ions, *J. Phys. B: At. Mol. Opt. Phys.* **42**, 195002 (2009).
- [14] R. Pal, M. S. Safronova, W. R. Johnson, A. Derevianko, and S. G. Porsev, Relativistic coupled-cluster single-double method applied to alkali-metal atoms, *Phys. Rev. A* **75**, 042515 (2007).
- [15] B. K. Mani, K. V. P. Latha, and D. Angom, Relativistic coupled-cluster calculations of ^{20}Ne , ^{40}Ar , ^{84}Kr , and ^{129}Xe : Correlation energies and dipole polarizabilities, *Phys. Rev. A* **80**, 062505 (2009).
- [16] H. S. Nataraj, B. K. Sahoo, B. P. Das, and D. Mukherjee, Reappraisal of the Electric Dipole Moment Enhancement Factor for Thallium, *Phys. Rev. Lett.* **106**, 200403 (2011).
- [17] R. Kumar, S. Chattopadhyay, B. K. Mani, and D. Angom, Electric dipole polarizability of group-13 ions using perturbed relativistic coupled-cluster theory: Importance of nonlinear terms, *Phys. Rev. A* **101**, 012503 (2020).
- [18] E. Eliav, U. Kaldor, and Y. Ishikawa, Transition energies of ytterbium, lutetium, and lawrencium by the relativistic coupled-cluster method, *Phys. Rev. A* **52**, 291 (1995).
- [19] E. Eliav, U. Kaldor, and Y. Ishikawa, Transition energies of mercury and ekamercury (element 112) by the relativistic coupled-cluster method, *Phys. Rev. A* **52**, 2765 (1995).
- [20] B. K. Mani and D. Angom, Fock-space relativistic coupled-cluster calculations of two-valence atoms, *Phys. Rev. A* **83**, 012501 (2011).
- [21] B. K. Mani and D. Angom, Atomic properties calculated by relativistic coupled-cluster theory without truncation: Hyperfine constants of Mg^+ , Ca^+ , Sr^+ , and Ba^+ , *Phys. Rev. A* **81**, 042514 (2010).

- [22] B. K. Mani, S. Chattopadhyay, and D. Angom, RCCPAC: A parallel relativistic coupled-cluster program for closed-shell and one-valence atoms and ions in FORTRAN, *Comput. Phys. Commun.* **213**, 136 (2017).
- [23] W. R. Johnson, *Atomic Structure Theory: Lectures on Atomic Physics* (Springer, Berlin, 2007).
- [24] A. K. Mohanty, F. A. Parpia, and E. Clementi, Kinetically balanced geometric Gaussian basis set calculations for relativistic many-electron atoms, in *Modern Techniques in Computational Chemistry: MOTECC-91*, edited by E. Clementi (Scientific and Engineering Computations, Kingston, New York, 1991).
- [25] P. Jönsson, G. Gaigalas, J. Bieroń, C. Froese Fischer, and I. P. Grant, New version: GRASP2K relativistic atomic structure package, *Comput. Phys. Commun.* **184**, 2197 (2013).
- [26] I. P. Grant and B. J. McKenzie, The transverse electron-electron interaction in atomic structure calculations, *J. Phys. B* **13**, 2671 (1980).
- [27] E. A. Uehling, Polarization effects in the positron theory, *Phys. Rev.* **48**, 55 (1935).
- [28] W. R. Johnson, I. Bednyakov, and G. Soff, Vacuum-Polarization Corrections to the Parity-Nonconserving $6s-7s$ Transition Amplitude in ^{133}Cs , *Phys. Rev. Lett.* **87**, 233001 (2001).
- [29] V. M. Shabaev, I. I. Tupitsyn, and V. A. Yerokhin, Model operator approach to the Lamb shift calculations in relativistic many-electron atoms, *Phys. Rev. A* **88**, 012513 (2013).
- [30] V. M. Shabaev, I. I. Tupitsyn, and V. A. Yerokhin, QEDMOD: FORTRAN program for calculating the model Lamb-shift operator, *Comput. Phys. Commun.* **189**, 175 (2015).
- [31] I. Grant, Relativistic atomic structure, in *Springer Handbook of Atomic, Molecular, and Optical Physics*, edited by G. Drake (Springer, New York, 2006), pp. 325–357.
- [32] NIST atomic spectroscopic database, 2013, https://physics.nist.gov/PhysRefData/ASD/levels_form.html.
- [33] E. A. Konovalova and M. G. Kozlov, Correlation, Breit, and QED effects in spectra of Mg-like ions, *Phys. Rev. A* **92**, 042508 (2015).
- [34] J. Mitroy, J. Y. Zhang, M. W. J. Bromley, and R. G. Rollin, Blackbody radiation shift of the Al^+ clock transition, *Eur. Phys. J. D* **53**, 15 (2009).
- [35] M. Stanek, L. Glowacki, and J. Migdalek, The spin-allowed and spin-forbidden $3s^2\ ^1S_0-3s3p\ ^1P_1, ^3P_1$ transitions in the magnesium isoelectronic sequence, *J. Phys. B: At. Mol. Opt. Phys.* **29**, 2985 (1996).
- [36] B. P. Das and M. Idrees, Some theoretical aspects of the group-IIIa-ion atomic clocks: Intercombination transition probabilities, *Phys. Rev. A* **42**, 6900 (1990).
- [37] H.-S. Chou, H.-C. Chi, and K.-N. Huang, Relativistic excitation energies and oscillator strengths including core-polarization effects for the intercombination and resonance transitions in Mg-like ions, *J. Phys. B: At. Mol. Opt. Phys.* **26**, 4079 (1993).
- [38] Y. Zou and C. F. Fischer, Multiconfiguration Dirac-Hartree-Fock optimization strategies for $3s^2\ ^1S_0-3s3p\ ^3P_1$ transition rates for $\text{Al}^+-\text{S}^{4+}$, *Phys. Rev. A* **62**, 062505 (2000).
- [39] U. I. Safronova, W. R. Johnson, and H. G. Berry, Excitation energies and transition rates in magnesiumlike ions, *Phys. Rev. A* **61**, 052503 (2000).
- [40] P. Jonsson and C. Froese Fischer, Accurate multiconfiguration Dirac-Fock calculations of transition probabilities in the Mg isoelectronic sequence, *J. Phys. B: At. Mol. Opt. Phys.* **30**, 5861 (1997).
- [41] W. R. Johnson, M. S. Safronova, and U. I. Safronova, Relativistic many-body calculations of energies of Mg I, Al II, Al I, Hg I, Tl II, Tl I, Pb I, Bi II and Bi I, *Phys. Scr.* **56**, 252 (1997).
- [42] W. M. Itano, J. C. Bergquist, A. Brusch, S. A. Diddams, T. M. Fortier, T. P. Heavner, L. Hollberg, D. B. Hume, S. R. Jefferts, L. Lorini, T. E. Parker, T. Rosenband, and J. E. Stalnaker, Optical frequency standards based on mercury and aluminum ions, in *Time and Frequency Metrology*, Vol. 6673, edited by R. J. Jones, International Society for Optics and Photonics (International Society for Optics and Photonics, Bellingham, Washington, 2007), pp. 9–19.
- [43] K. Beloy, D. R. Leibrandt, and W. M. Itano, Hyperfine-mediated electric quadrupole shifts in Al^+ and In^+ ion clocks, *Phys. Rev. A* **95**, 043405 (2017).
- [44] B. C. Johnson, P. L. Smith, and W. H. Parkinson, Transition probability of the Al II 2669 intersystem line, *Astrophys. J.* **308**, 1013 (1986).
- [45] J. A. Kernahan, E. H. Pinnington, J. A. O'Neill, R. L. Brooks, and K. E. Donnelly, Radiative lifetime measurements in Al II-VII, *Phys. Scr.* **19**, 267 (1979).
- [46] Y. Baudinet-Robinet, P. D. Dumont, H. P. Garnir, E. Biémont, and N. Grevesse, Beam-foil study of Al II-VI between 1110 and 1900 Å, *J. Phys. Colloques* **40**, C1–175 (1979).
- [47] H. G. Berry, J. Bromander, and R. Buchta, Some mean life measurements in the Na I and Mg I isoelectronic sequences, *Phys. Scr.* **1**, 181 (1970).
- [48] P. Shorer, C. D. Lin, and W. R. Johnson, Oscillator strengths for the magnesium isoelectronic sequence, *Phys. Rev. A* **16**, 1109 (1977).
- [49] S. Chattopadhyay, B. K. Mani, and D. Angom, Triple excitations in perturbed relativistic coupled-cluster theory and electric dipole polarizability of group-IIb elements, *Phys. Rev. A* **91**, 052504 (2015).
- [50] S. Chattopadhyay, B. K. Mani, and D. Angom, Electric dipole polarizability of alkaline-earth-metal atoms from perturbed relativistic coupled-cluster theory with triples, *Phys. Rev. A* **89**, 022506 (2014).
- [51] V. M. Shabaev, K. Pachucki, I. I. Tupitsyn, and V. A. Yerokhin, QED Corrections to the Parity-Nonconserving $6s-7s$ Amplitude in ^{133}Cs , *Phys. Rev. Lett.* **94**, 213002 (2005).
- [52] V. M. Shabaev, I. I. Tupitsyn, K. Pachucki, G. Plunien, and V. A. Yerokhin, Radiative and correlation effects on the parity-nonconserving transition amplitude in heavy alkali-metal atoms, *Phys. Rev. A* **72**, 062105 (2005).